Volcanism from an active continental collision zone: A case study on most recent lavas within Turkish-Iranian plateau

Monireh Kheirkhah[1*], Hassan Mirnejad[2]

1- Research Institute for Earth Sciences, Geological Survey of Iran, Tehran, Iran
2- Department of Geology, Faculty of Science, University of Tehran, Tehran, Iran

* Corresponding Author: monireh.kheirkhah@yahoo.com

Abstract

Voluminous Quaternary extrusive rocks, associated with widespread volcanic activities, occur in the northwestern Iran and across the Turkish-Iranian plateau. Field and petrographic studies reveal that these volcanic rocks, consisting of basalt to trachyandesite, occur as lava flows, columnar basalts, and cinder cones in three distinct areas of northern (Bazergan-Maku-Burlan), middle (Chalderan) and southern (Tazehshahr) regions. Sr and Nd isotope compositions show that the parental magmas to these rocks originated from subduction-modified lithospheric mantle source. However, the volcanic rocks from middle and southern areas are characterized by having higher abundances of incompatible element relative to those from northern area. The formers have also higher $^{87}Sr/^{86}Sr$ and lower $^{143}Nd/^{144}Nd$ ratios relative to the latter. These geochemical features, along with the field observations and petrography, indicate that the magmas for the middle and southern areas underwent some degrees of crustal contamination in their source region.

Keywords: Volcanic Rocks, Lithosphere, Crustal Contamination, Northwest Iran.

1– Introduction

The Quaternary magmatism in northwest (NW) of Iran and eastern Turkey is related to the slab break-off or lithospheric delamination event across the Bitlis –Zagros suture zone (Kheirkhah *et al*., 2009). The collision between the Eurasian and Arabian plate along this suture zone was the consequence of the closure of Southern Neo-Tethys Ocean around 25-30 Myr (McQuarrie and van Hinsbergen, 2013). Pleistocene to recent volcanic activity across Eastern Anatolia was studied by Pearce *et al*. (1990). However, few detailed studies have been carried out on petrography, major, trace elements and isotope ratios of the young volcanic rocks in NW Iran. These rocks crop out is three different zones of northern (Burlan-Bazergan-Maku), middle (Chalderan), and southern (Tazehshahr) (Fig. 1). The principal aims of this research are to describe the eruptive styles, petrography, geochemical compositions and finally their petrogenesis.

2– Geological setting

The Quaternary volcanic rocks occurring in the NW of Iran are part of Alpine –Himalayan orogenic system and the Turkish-Iranian Orogenic Plateau. They are situated at 38°-39°50´ East and 44°- 45° North (Fig. 1). The basement rocks in NW Iran are characterized by Precambrian metamorphic complexes derived from northern Gondwanaland, which includes schist, siltstone, carbonate and dolomite-bearing low-grade metamorphic (Alavi M. 1996). These are overlain by an Ordovician sequence which consists of schist, slate and phyllite, all of which are in turn overlain by Silurian volcano-sedimentary rocks (Alavi M., 1996). The latter are covered by quartzite, dolomite and sandstone of the Late Devonian–Early Carboniferous. Permian limestone conformably covers the Carboniferous sequence. Mesozoic rocks consist of sandstone, limestone and conglomerate of Triassic–Cretaceous age which are overlain by limestone, conglomerate and volcanic rocks (basalts, andesite, and dacite) of Eocene. Eocene deposits are covered uncomfortably by Oligocene-Miocene Formation of Quaternary alluvium components which consist of conglomerate, sandstone, limestone and travertine. According to Kheirkhah *et al*. (2009) the Eocene igneous rocks are related to lithospheric delamination in the region.

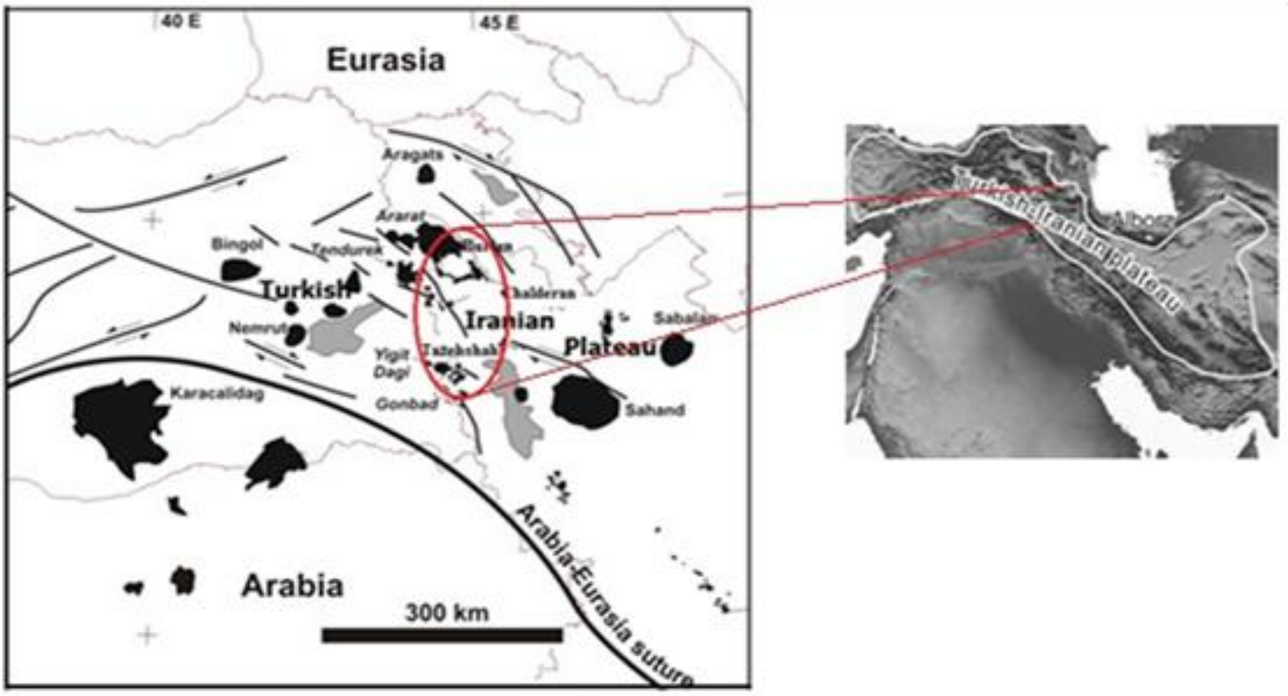

Figure 1) Quaternary volcanic centres (black) and major faults in Turkish –Iranian plateau. Grey areas are lakes (Modified from Kheirkhah et al., 2009).

The Quaternary volcanic rocks in NW Iran cover an area of almost 600 km^2 and stretch across the political borders of Turkey, Azerbaijan, and Armenia. These rocks crop out in three distinct areas: the northern (Burlan-Bazergan-Maku), middle (Chalderan) and southern (Tazehshahr) sectors (Fig. 1). The lava flows of the northern area originated from little Ararat volcanoes. A few basaltic lavas were derived from small fissure ridge in the Maku area. These lava flows represent ropy (Fig. 2A), tumulus (Fig. 2B), aa (Fig. 2C) and pahoehoe structures. Some ash and scoria deposits are found in the north of Bazergan. Several structures of columnar basalts in middle area (Chalderan) (Fig. 2D) and isolated cinder cones and craters in southern area (Tazehshahr) represent fissure–type eruptions within pull-apart basin zones. Strike–slip faults with NW-SE trend in pull-apart basin indicate a band of oblique normal and strike–slip deformation within the middle and southern areas (Copley and Jackson, 2006; Kheirkhah *et al*., 2009).

3– Petrography

The Quaternary volcanic rocks in the NW Iran are characterized by alkali and subalkali olivine basalts that exhibit hyaline, hyalo- microlitic, trachytic, porphyritic, intersertal and intergranular textures. Phenocrysts are mainly plagioclase ± olivine ± clinopyroxene ± amphiboles. The main phenocrysts of basaltic rocks from the northern sector are plagioclase + olivine ± clinopyroxene with dendritic, skeletal, spiky and swallow-tail crystals (Fig. 3A). In Maku area, there are some basaltic rocks with intersertal texture.

Table 1) Major oxide (wt.%), trace element (ppm) and isotope contents of volcanic rocks from northwest Iran.

	Chalderan	Chalderan	Chalderan	Chalderan	Chalderan*	Chalderan*	Tazehshahr
Samples	MA-40	MA-42.1	MA-41	MA-43.2	Mu-11.16	Mu-12.17	SA-15
SiO_2	55.37	51.41	52.62	53.05	50.43	50.1	49.63
TiO_2	1.91	1.78	1.33	1.78	2.21	2.05	1.11
Al_2O_3	15.53	15.41	15.86	14.47	17.72	17.91	13.55
MnO	0.15	0.15	0.1	0.15	0.17	0.181	0.12
MgO	3.69	3.37	4.92	3.22	3.85	4.21	5.91
CaO	7.2	7.28	9.02	8.02	7.06	7.37	7.17
Na_2O	5.05	5.14	3.54	4.81	5.61	5.39	1.69
K_2O	1.53	1.73	2.66	1.72	1.586	1.629	3.91
P_2O_5	0.71	0.69	0.76	0.67	0.764	0.746	0.17
FeO	4.58	6.03	4.36	5.47			7.25
Fe_2O_3	3.41	3.28	2.83	3.28	11.52	11.71	2.61
Total	99.13	96.27	98	96.63	100.47	100.25	93.12
Ba	449	405	267	407	435.1	567.3	530
Rb	49	54	62	53	20	25	
Sr	549	657	822	755	580.7	651.8	
Cs	1.37	1.17	0.87	1.7	0.1	0.5	0.6
Ga	11.41	16.69	8.72	17.77	20.8	20.5	
Ta	0.16	0.94	1.71	1.08	1.27	1.29	1.3
Nb	10.6	17.3	12.8	18	26.9	26.6	
Hf	0.86	10.96	7.58	1.15	5.79	5.91	
Zr	219	254	207	260	268.2	299.6	
Y	25	33	30	34	37.7	38.3	
Th	1.46	2.15	4.56	2.14	4.7	5.7	
Cr	52	58	280	59	6.8	1.9	36
Ni	43	42	122	46	21.1	22.5	79
Co	36	34.9	25.7	34.7	29.1	32.3	23
Sc	17	15	19	18	14	12	19
V	277	260	200	260	187.9	168.8	110
Pb	-0.9	5.2	8.2	7.4	9.7	10.6	
Zn	98.9	111.1	57.4	111.2	131.3	130.5	58
La	59	56	66	57	37.1	39.9	43
Ce	38	44	58	47	73.5	78.47	61
Nd	26	32	29	37	38.5	39.9	24
Sm	3.9	4	4.6	3.9	7.49	7.72	5.4
Eu	1.24	1.26	1.39	1.19	2.18	2.24	1.2
Gd					7.14	7.14	
Tb	0.66	0.88	0.94	0.87	1.1	1.1	1.3
Tm					0.54	0.55	
Yb	2.25	2.38	3.24	2.33	3.31	3.41	2.3
As					4.9	5.7	
U					0.6	1.4	
Pr					9.41	9.9	
Dy					6.36	6.41	
$^{87}Sr/^{86}Sr$					0.705705	0.7056	
$^{143}Nd/^{144}Nd$					0.512708	0.51269	

Table 1) Continued

	Tazehshahr	Tazehshahr	Tazehshahr	Tazehshahr*	Tazehshahr*	Tazehshahr*	Tazehshahr*
Samples	SA-39	SA-4	SA-45	Mu-13.18	Mu-14.19	Mu-15.20	Mu-15.21
SiO_2	49.74	52.99	52.11	49.03	52.21	48.11	48.71
TiO_2	1.72	1.14	1.23	1.44	1.23	1.32	1.19
Al_2O_3	14.54	14.59	16.11	14.74	16.02	13.74	13.79
MnO	0.16	0.12	0.13	0.117	0.13	0.14	0.14
MgO	8.14	7.01	5.76	6.16	6.58	11.46	9.92
CaO	9.15	8.83	7.76	12.31	8.67	9.64	9.96
Na_2O	2.39	1.94	3.34	3.54	4.24	3.4	3.75
K_2O	2.11	2.12	2.22	1.361	2.73	2.01	2.22
P_2O_5	0.88	0.72	0.21	0.8	0.57	0.76	0.73
FeO	6.62	5.18	5.95				
Fe_2O_3	3.22	2.64	2.73	8.65	7.48	8.99	8.26
Total	98.67	97.28	97.55	97.58	99.37	100	100.18
Ba	576	490	531	760.6	722.03	799	810
Rb				8.7	64.68	47	58
Sr				1724.1	839.49	1113	1125
Cs	1.1	0.73	0.85	2.1	3.69	1.6	
Ga				16.5	17.02	15.5	
Ta	0.57	0.69	0.82	1.12	1.75	1.8	
Nb				22.7	31.56	33	32
Hf				3.59	4.5	4.09	
Zr				170.6	211.19	191	203
Y				26.8	24.32	24	24
Th				6.7	17.3	8.91	8
Cr	42	98	118	254.8	190.47	518	439
Ni	150	69	134	169.5	109.74	354	243
Co	15	69	52	28.2	29.91	48	
Sc	16	13	20	18.3	15.91	21	23
V	68	100	230	138.7	147.4	160	144
Pb				13.2	13.68	8.96	
Zn	19	345	300	73.8	71.71	78.2	
La	39	36	41	54.8	61.94	66.11	72
Ce	46	50	38	108.17	111.26	125.94	
Nd	31	26	28	52.5	44.92	54.33	53
Sm	5.3	5.1	4.3	8.5	7.06	8.18	
Eu	2.2	1.7	1.4	2.3	1.81	2.12	
Gd				6.39	5.19	5.68	
Tb	1.1	1.4	1.4	0.87	0.77	0.8	
Tm				0.34	0.33	0.31	
Yb	1.5	2.4	2.6	2.15	2.04	1.89	
As				3.5	1.41	2.25	
U				1.8	3.06	2.25	15
Pr				13.51	12.55	14.81	
Dy				4.71	4.27	4.34	
$^{87}Sr/^{86}Sr$				0.705008	0.705338	0.704979	
$^{143}Nd/^{144}Nd$				0.512753	0.51263	0.512627	

Table 1) Continued

	Tazehshahr*	Burlan*	Burlan*	Burlan	Burlan	Burlan	Burlan
Samples	Mu-15.22	Mu16.23	Mu-6.11	MA-21	MA-9	Mk-11	Mk-21
SiO_2	59.17	46	52.45	51.49	52.17	50.9	51.83
TiO_2	0.81	1.5	1.27	1.31	1.39	1.33	1.38
Al_2O_3	16.03	14.78	16.15	15.84	15.85	15.8	14.17
MnO	0.09	0.16	0.143	0.15	0.14	0.14	0.13
MgO	2.23	8.47	6.68	6.62	5.87	7.94	7.71
CaO	5.59	11.43	8.1	8.26	8.51	9.04	8.28
Na_2O	4.78	3.94	4.16	3.18	2.13	3	3.41
K_2O	3.93	1.99	0.994	0.95	1.13	0.86	1
P_2O_5	0.59	0.81	0.257	0.23	0.29	0.25	0.23
FeO	2.16			5.74	5.92	5.51	5.34
Fe_2O_3	4.71	9.47	9.03	2.81	2.89	2.83	2.88
Total	99.94	99.79	99.23	96.57	96.28	97.59	96.34
Ba	940	851	288.1	259	284	235	236
Rb	128	44	19.5	52	47	52	45
Sr	916	1066	364.4	387	385	400	404
Cs		3.8	2.2	0.69	0.41	0.77	0.89
Ga		16.3	18.4	13.4	15.45	10.26	10.44
Ta		1.69	0.58	1.04	0.92	1.15	0.93
Nb	37	33	9.3	7.4	9.5	10.3	9.5
Hf		3.9	3.33	5.41	1.98	6.12	5.41
Zr	252	184	149.1	143	145	146	143
Y	20	28	25	25	26	27	23
Th	21	11.3	3	2.1	1.81	1.86	1.83
Cr	14	295	223	259	248	215	205
Ni	8	167	148	117	120	100	99
Co		40.6	37.1	33.4	34.3	34.3	33.9
Sc	8	32	21.7	22	25	21	21
V	74	198	165.2	198	207	186	184
Pb		9.49	9.5	7.8	9.6	8.9	8.8
Zn		82.3	74.9	78.5	81.4	76.7	72.4
La	73	61.25	16.8	25	29	27	25
Ce		113.7	31.85	25	20	41	37
Nd	47	49.49	17.5	11	14	13	11
Sm		7.92	3.98	3.8	3.3	4.9	4.2
Eu		2.15	1.29	1.2	1	1.23	1.03
Gd		6.19	4.45				
Tb		0.89	0.72	0.77	0.9	0.47	0.84
Tm		0.23	0.36				
Yb	1.7	2.29	2.25	3.2	3.2	3.01	2.98
As			-1.6				
U	32	2.34	1.1				
Pr		13.39	4.11				
Dy		4.97	4.2				
$^{87}Sr/^{86}Sr$		0.70557	0.704452				
$^{143}Nd/^{144}Nd$		0.512643	0.512832				

Table 1) Continued

	BM*	BM*	BM*	BM*	BM*	BM*	BM*
Samples	Mu-10.15	Mu-17.24	Mu-18.25	Mu-3.9	Mu-5.10	Mu20-26	Mu-2.1
SiO_2	50.35	51.4	48.95	50.19	49.81	49.64	50.38
TiO_2	1.54	2.17	1.6	1.9	1.77	1.67	1.76
Al_2O_3	16.44	16.93	16.37	17.16	16.95	16.09	17.1
MnO	0.16	0.162	0.142	0.16	0.15	0.159	0.147
MgO	7.57	5.31	5.16	5.3	6.1	6.93	6.01
CaO	8.7	8.11	10.61	8.42	9.1	9.14	8.65
Na_2O	4.5	5.02	4.49	4.92	4.65	4.51	4.83
K_2O	1.029	0.682	0.55	0.64	0.71	1.055	0.787
P_2O_5	0.442	0.315	0.264	0.276	0.35	0.416	0.38
FeO	6.17						
Fe_2O_3	3.04	10.41	8.86	10.18	9.63	9.84	9.59
Total	99.95	99.84	96.42	98.47	98.58	98.78	100.46
Ba	323	229.3	213.1	171.2	174.6	309.3	271
Rb	16	10.4	7.1	9.4	10.8	14.6	10.3
Sr	658	460.4	522.6	491.6	518.6	571.2	564
Cs	-0.1	-2.7	0.2	0.9	0.9	0.3	
Ga	19.1	19.5	17.3	21.3	18.9	18.9	19.7
Ta			0.33			0.66	
Nb	14.9	7	5.4	8.2	11.2	12.2	8.6
Hf			3.64			3.71	
Zr	179.2	234.4	171.7	210.6	203.7	171.7	197
Y	30.8	37	27.1	31.2	27.5	29.2	31.5
Th	6.9	2.5	1.5	7.5	5.8	2.1	7.1
Cr	211.3	40.8	42.7	35.7	116.2	197.4	106.9
Ni	97.5	38.8	58.6	39.4	65.6	155.7	62.4
Co	38.4	37.1	33.4	33.3	36.6	39.2	35.7
Sc	22.5	31.7	19.6	26.3	25.3	23.2	20.5
V	177.6	180.7	154.6	146.4	152.7	183.9	159.4
Pb	0.8	5.1	3.2	4	3.8	4.4	2.4
Zn	73.5	77.7	73.7	62.6	71	85.8	65.9
La	27.3	14.7	11.1	14.7	16.2	20.8	15
Ce			26.05			43.98	
Nd	26.2	26.5	17.3	23.2	21.6	24.3	20
Sm			4.19			5.19	
Eu			1.46			1.66	
Gd			4.84			5.47	
Tb			0.78			0.85	
Tm			0.39			0.43	
Yb			2.4			2.61	
As	2.4	4.2	4.2	8.7	1.8	0.3	
U	-0.6	2.4	0.8	0.4	-1.3	0.6	2
Pr			3.74			5.81	
Dy			4.57			4.94	
$^{87}Sr/^{86}Sr$			0.704657			0.704461	
$^{143}Nd/^{144}Nd$			0.512923			0.512832	

Table 1: Major oxide (wt.%) , trace element (ppm) and isotope contents of volcanic rocks, * Samples analyzed by and reported in Kheirkhah et al (2009).

Some of the micro-phenocrysts of clinopyroxene with spiky form fill spaces within other minerals. Fern-like pyroxene and spiky plagioclase crystals were formed in response to rapid cooling of the lavas. In some of basalts and trachybasalts, most of the plagioclases and pyroxenes show reverse zoning and reaction rims (Fig.3B).

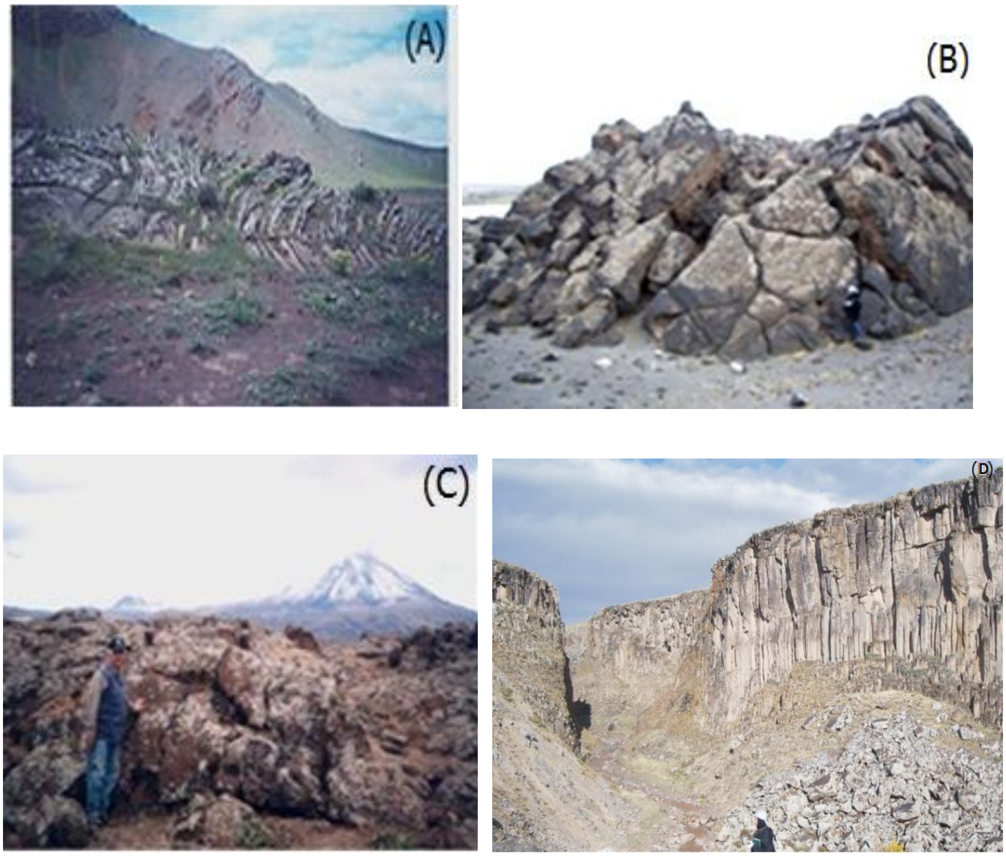

Figure 2) Field photos showing: A) ropy, B) tumulus, C ,) aa structures near Ararat, D) columnar basalts in Chalderan.

In the basaltic and trachyandesitic rocks from the middle and southern sectors of the study area, clinopyroxene + plagioclase ± olivine ± amphibole ± biotite phenocrysts reside in a fine-grained matrix consisting of pyroxene and K-feldspar. Some xenocrysts of quartz with reaction rims are also found (Fig. 3C) which show crustal contamination. In some of the basaltic rocks, which are situated in southern area (Tazehshahr), two different glassy matrixes (Fig. 3D).

4– Analytical methods

Major and selected trace elements for 18 samples were analyzed by Philips PW1400 X-Ray (XRF) spectrometer with a Rhodium (Rh) tube, at the Department of Geology, University of Leicester, UK (Kheirkhah *et al*., 2009). Major elements were analyzed on fused beads while trace elements on pressed powder briquettes. Full analytical procedures are given in Tarney and Marsh (1991). A subset of ten samples were analyzed for additional trace elements by Inductively Coupled Plasma Mass Spectroscopy (ICP-MS), using a Perkin Elmer-Sciex Elan 6000 in the Department of Earth Sciences at the University of Durham, following a standard nitric and hydrofluoric acid digestion (Ottley *et al*., 2003). Additional 21 samples were analyzed at the Geological Survey of Iran, Tehran, on a Philips model PW4000 XRF spectrometer.

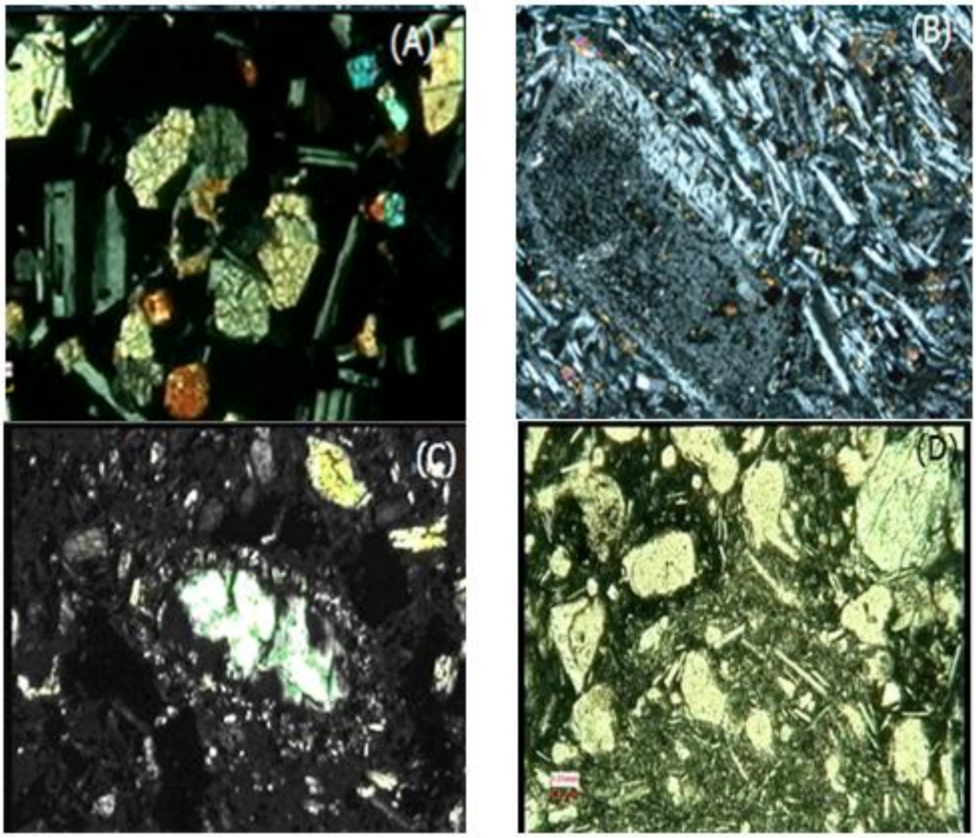

Figure 3) Microphotographs that show: A) hyalo porphyritic basalt with swallow-tail forms of plagioclase in Burlan, B) basaltic lava with reverse zoning of plagioclase in Maku, C) hyalo microlitic porphyritic basalt in Chalderan that show quartz surrounded by spiky pyroxenes as reaction rims, D) basalt from Tazehshahr illustrating plagioclase microliths and glass in its matrix.A,B,C Photographs are taken in XPL.

Nine samples were also analyzed for Rb-Sr and Sm-Nd isotope ratios at the Department of Earth Sciences, University of Durham, using a Thermo Electron Neptune Multi-collector Plasma Mass Spectrometer. The average $^{143}Nd/^{144}Nd$ value for pure and Sm-doped J & M standard was 0.511111±0.000008 (16ppm 2SD; n=16) (single run session). Sample data are reported relative to a J & M value of 0.511110. The average $^{87}Sr/^{86}Sr$ value for standard NBS987 was 0.710261±0.000007 (10ppm 2SD; n=9) (single run session). Sample data are reported relative to an NBS 987 value of 0.71024 (0.000021 subtracted from each sample). More details can be found in Kheirkhah *et al* (2009).

5– Geochemistry

Based on petrographic studies, a total of 39 fresh samples representing the various rocks types in the study area were analyzed for major, trace and isotope elements contents (Table 1).

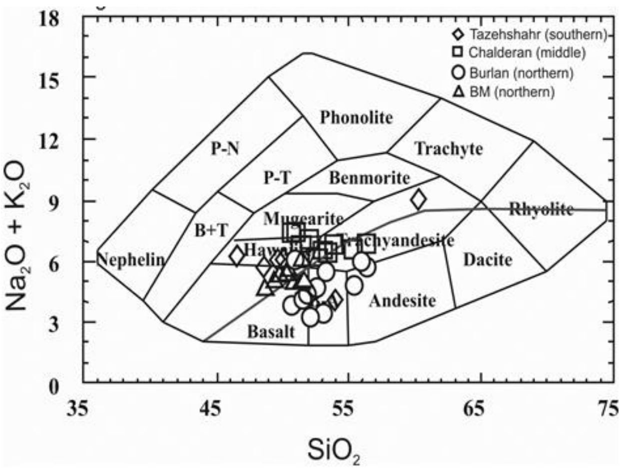

Figure 4) Total alkali versus silica diagram for volcanic rocks of NW Iran. After Cox et al (1978). The dividing line between alkalic and sub-alkalic magma series is from Miyashiro (1978).

The volcanic basic rocks cover a broad compositional spectrum from basalts to trachyandesite, with SiO_2 contents ranging between 46 to 59.17wt%. The Mg# varies between 37.03 (Chalderan) to 67.37 (Tazehshahr). The volcanic samples of the area lie in the fields of basalt, andesite, hawaiite, mugearite, trachyandesite and basaltic andesite, on the basis of total alkali vs. silica contents (Fig.4). Most samples plot on sub-alkaline field, with two samples from middle area (Chalderan) resides in the sub alkalic field (Fig.4). On the Harker variation diagrams, TiO_2, FeO, MnO, MgO, CaO show negative correlation with SiO_2, (Fig. 5), while K_2O and Na_2O do not exhibit any correlation with SiO_2.

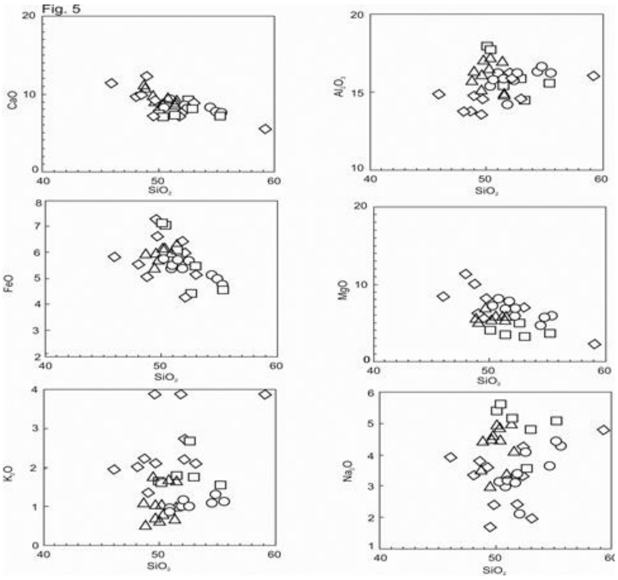

Figure 5) Harker diagrams illustrating the variation of major elements with increasing SiO_2 for the Quaternary volcanic rock from NW Iran. Symbols as in Fig. 4.

Sr–Nd isotopic ratios of volcanic rocks from NW of Iran are listed in Table 1. The samples of northern area have low $^{87}Sr/^{86}Sr$ ratios (0.704452–0.704657) and high ratios of $^{143}Nd/^{144}Nd$ (0.512832–0.512923), whereas those from the middle and southern area contain high $^{87}Sr/^{86}Sr$ ratios (0.704979–0.705705) and low $^{143}Nd/^{144}Nd$ ratios (0.512627–0.512753). All of the samples are situated within the mantle array close to Bulk Silicate Earth (BSE) on the $^{143}Nd/^{144}Nd$ vs. $^{87}Sr/^{86}Sr$ plot (Fig. 8). The volcanic rocks of northern area plot in the depleted quadrant, while those of Chalderan and Tazehshahr reside close to the enriched quadrant (Fig. 8).

6– Discussion

As it is discussed below, the variations in trace element contents in the suite of igneous rocks from the study area suggest that source contamination was an important process in changing the composition of magma. The normalized trace element patterns which show distinctive spikes, and peaks at Ba,Th and La could be associated with crustal contamination. To show the effect of crustal contamination, elemental ratio-ratio plots are normally used.

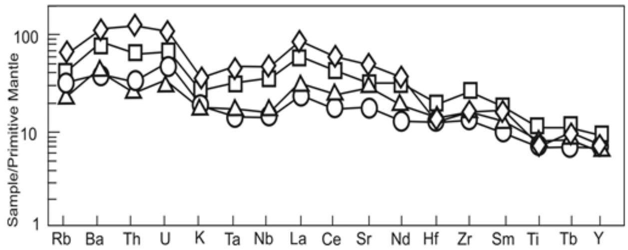

Figure 6) Primitive mantle normalized trace element pattern for volcanic rocks from NW Iran. Normalizing values are after Nakamura (1974). Symbols as in Fig. 4.

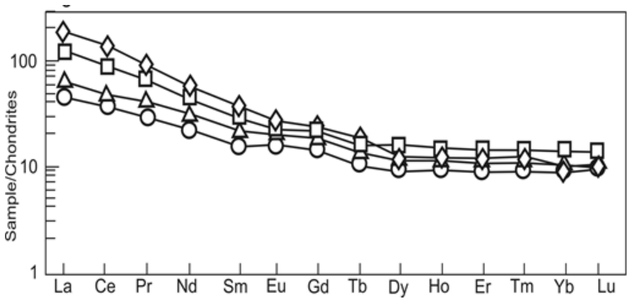

Figure 7) Chondrite normalized REE patterns for volcanic rocks from NW Iran. Normalizing values after McDonough and Sun (1995). Symbols as in Fig. 4.

On the primitive mantle normalized diagrams of McDonough and Sun (1995) (Fig. 6), samples from southern and middle areas have higher contents of incompatible elements that reflect incorporation of these elements during crustal contamination. In addition, volcanic rocks from southern and middle areas show more enrichment in light rare earth element (LREE) compared to those northern area (Fig. 7), all of which may be explained by partitioning of these elements into the melt during source contamination. In addition, Nb-Ta anomalies in the samples (Fig. 6) point to a subduction-modified (lithospheric) mantle source and the HREE distributions (Fig. 7) indicate melting in the shallow upper mantle in the spinel peridotite facies. It is thus likely that melting took place at the base of the lithospheric mantle where it was being heated by upwelling asthenosphere following slab breakoff.

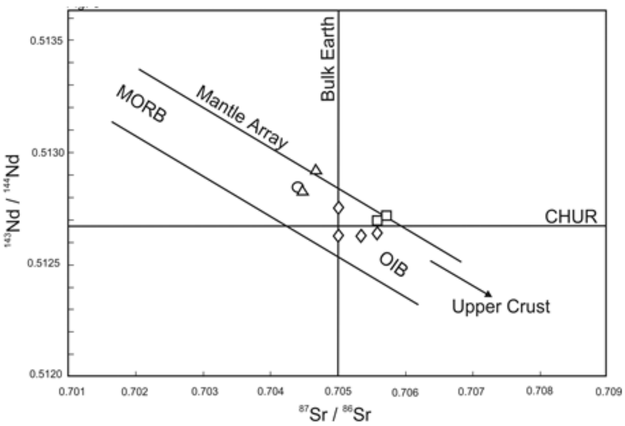

Figure 8) Sr-Nd isotope diagram for the NW Iran volcanic samples. Symbols as in Fig. 4.

On the Nd vs. Sr isotope diagram (Fig. 8), it is clear that contamination by continental crust have an important role in increasing $^{87}Sr/^{86}Sr$ and decreasing $^{143}Nd/^{144}Nd$ ratios for the southern and middle volcanic rocks. In contrast, samples from the northern area have the lowest $^{87}Sr/^{86}Sr$ and highest $^{143}Nd/^{144}Nd$ ratios and plot in the depleted quadrant (Fig. 8). This combined with the elemental abundances of these samples, suggests that parental magma for volcanic rocks in the northern area originated from a less enriched parts of lithospheric mantle source. Magmas for southern and middle areas also originated from the same lithospheric mantle source, but their Sr and Nd isotope ratios were modified due to enrichment in their sources. As it was mentioned above, such process also affected the incompatible trace elements of these samples.

7– Conclusions

In northwestern of Iran (Turkish–Iranian plateau), widespread outcrops of Quaternary basalt to trachyandesite are found in three distinct areas, namely northern (Burlan-Bazergan-Maku), middle (Chalderan) and southern (Tazehshahr). The volcanic rocks from northern area are characterized by lower abundances in incompatible elements relative to those in southern and middle areas. In addition, the $^{87}Sr/^{86}Sr$ and $^{143}Nd/^{144}Nd$ ratios are different between these areas, so that the volcanic rocks from northern area plot in the depleted quadrant while those from middle and southern area plot in the more enriched parts on the Nd *vs.* Sr isotope diagram. These variations in major and trace element contents as well as isotope ratios indicate that magmas for the volcanic rocks were derived from a lithospheric mantle, but those from the middle and southern areas were modified by crustal contamination process in their sources. Melting in the lithospheric mantle was induced by heat released during upwelling of asthenosphere materials following slab breakoff.

Acknowledgments:

The author would like to thank Dr. A. Torkian and an anonymous reviewer for their kind and careful comments that made the manuscript improved. The author is indebted to Dr. Mohammad Hashem Emami for his help during this research and she is extremely grateful to Dr. Mark Allen, Reader in Tectonic at Durham University for his useful comments and help on the geochemical analyses during the course of this research. The author would like to thank the Geological Survey of Iran, particularly Mr. Korei and Dr. Ghorashi, for providing support during the field works. This work was funded by the Geological Survey of Iran and the Durham work was funded by Research Grant R050475 from University of Durham, UK.

References:

Alavi, M., 1996. Tectonostratigraphic synthesis and structural style of the Alborz mountain system in northern Iran. Journal of Geodynamics: 21, 1–33.

Copley, A., Jackson, J. 2006. Active tectonics of the Turkish-Iranian plateau. Tectonics: 25, TC6006.

Cox, K. G., Bell, J. D., Pankhurst. R. J. 1979. The interpretation of igneous rocks, London, George Allen and Unwin, 450pp.

Kheirkhah, M., Allen, M. B., Emami, M. 2009. Quaternary Syn-Collision Magmatism from the Iran/Turkey borderlands. Journal of Volcanology and Geothermal Research: 182, 1–12.

McDonough, W. F., Sun, S. S. 1995. Composition of the Earth. Chemical Geology: 120, 223–253.

McQuarrie, N., van Hinsbergen, D. J. 2013. Retro-deforming the Arabia-Eurasia collision zone: Age of collision versus magnitude of continental subduction. Geology: 41, 315–318.

Ottley, C. J., Pearson, D. G., Irvine, G. J. 2003. A routine method for the dissolution of geological samples for the analysis of REE and trace elements via ICP- MS. In: Holland, J.G., Tanner, S.D. (Eds.), Plasma Source Mass Spectrometry: Applications and Emerging Technologies. Royal Society of Chemistry, Cambridge, pp. 221–230.

Pearce, J. A., Bender, J. F., Yilmaz, T., Moorbath, S., Mitchell, J. G. 1990. Genesis of collision volcanism in eastern Anatolia, Turkey. Journal of Volcanology and Geothermal Research: 44, 189–229.

Tarney, J., Marsh, N. 1991. Major and trace element geochemistry of Holes CY-1 and CY-4: Implications for petrogenetic models. In: Gibson, I.I., Malpas, J., Robinson, P.A, Xenophonotos, C. (Eds.), Initial Reports, Holes CY-1 and CY-1A. Geological Survey of Canada, pp. 133–175.

Received: 20 November 2013 / Accepted: 28 March 2014 / Published online: 15 April 2014

Dr. Lenka Findoráková
Institute of Geotechnics, Slovak Academy of Sciences, Watsonova 45,043 53 Košice, Slovak Republic
E–Mail: findorakova@saske.sk

Dr. Mohamed Omran M. Khalifa
Geology Department, Faculty of Science, South Valley, Qena, 83523, Egypt
E–Mail: mokhalifa@svu.edu.eg

Prof. A. K. Sinha
D.Sc. (Moscow), FGS (London). B 602, VigyanVihar, Sector 56, GURGAON 122011, NCR DELHI, Haryana
E–Mail: anshuksinha@gmail.com